

Probing Diverse Disulfur Ligands in the Mo₂Sn- /0 (n = 4 ~8) Clusters: Structural Evolution and Chemical Bonding (Postprint)

Authors: ZHANG Xiao-Fei, LIU Xiu-Juan, XU Ruo-Nan, WU Ni, HUANG Xin, WANG Bin

Date: 2017-11-05T00:00:00+00:00

Abstract

Density functional theory (DFT) and coupled cluster theory (CCSD(T)) calculations were employed to investigate the geometric and electronic structures of a range of dinuclear molybdenum sulfide clusters, Mo₂Sn- and Mo₂Sn (n = 4~8). The results showed that the sulfur atoms tended to occupy the terminal sites of the clusters continuously in the process of sequential sulfidation. After the oxidation state of Mo atoms reached the maximum of +6, diverse disulfur ligands emerged in the sulfur-rich Mo₂Sn-/0 (n = 7, 8) clusters. The driving forces of removing a sulfur atom from different S ligands in Mo₂Sn-/0 (n = 4~8) clusters, especially from those disulfur units, were evaluated. The corresponding order may provide insight into the pretreatment of fresh MoS₂ catalysts. Vertical detachment energies (VDEs) were predicted according to the Generalized Koopmans' theorem, and then the photoelectron spectra (PES) were simulated. Molecular orbital and spin density values were analyzed to elucidate the chemical bonding and the evolutionary behavior in the dinuclear molybdenum sulfide clusters.

Full Text

Probing Diverse Disulfur Ligands in the Mo S / (n = 4-8) Clusters: Structural Evolution and Chemical Bonding

ZHANG Xiao-Fei (张晓菲), LIU Xiu-Juan (刘秀娟), XU Ruo-Nan (徐若男), WU Ni (吴妮), HUANG Xin (黄昕), WANG Bin (王彬)

Department of Chemistry, Fuzhou University, Fuzhou 350116, China

ABSTRACT

Density functional theory (DFT) and coupled cluster theory (CCSD(T)) calculations were employed to investigate the geometric and electronic structures of a range of dinuclear molybdenum sulfide clusters, Mo_2S_n and $\text{Mo}_2\text{S}_{n-1}$ ($n = 4-8$). The results showed that sulfur atoms tended to occupy terminal sites continuously during sequential sulfidation. After the oxidation state of Mo atoms reached the maximum of +6, diverse disulfur ligands emerged in the sulfur-rich Mo_2S_n ($n = 7, 8$) clusters.

The driving forces for removing a sulfur atom from different S ligands in Mo_2S_n ($n = 4-8$) clusters, especially from those disulfur units, were evaluated. The corresponding order may provide insight into the pretreatment of fresh MoS catalysts. Vertical detachment energies (VDEs) were predicted according to the Generalized Koopmans' theorem, and photoelectron spectra (PES) were simulated. Molecular orbital and spin density analyses were performed to elucidate the chemical bonding and evolutionary behavior in the dinuclear molybdenum sulfide clusters.

Keywords: molybdenum sulfide; gas-phase cluster; density functional theory; polysulfido (S_n) ligand; simulated photoelectron spectrum

1. INTRODUCTION

Molybdenum sulfide has attracted intense attention due to its wide applications in mechanical treatments, catalysis, energy materials, and other fields [1-8]. In catalysis, molybdenum sulfide serves as a promising low-cost alternative to platinum and other noble metal catalysts for the hydrogen evolution reaction (HER) [9-14]. Additionally, MoS₂-based catalysts are widely used in petroleum refining [15], including hydrodesulfurization (HDS) and hydrodenitrogenation (HDN) reactions. Considerable attention has been devoted to studying the active sites in these catalysts [16-25]. It is generally accepted that sulfur vacancies (or coordination unsaturated sites, CUS) in MoS₂ are the key active centers [26, 27]. However, Besenbacher et al. [22] also proposed that specific brim sites without sulfur vacancies contribute to HDS activity. Furthermore, Vrabel et al. [11] showed that reduced molybdenum sulfides containing disulfide ligands appear to be catalytically active. Several molybdenum complexes containing various S ligands have been synthesized recently and are considered capable of mimicking MoS₂ edge sites for catalytic hydrogen generation [28-31]. Despite this progress, more detailed studies on the active sites of molybdenum sulfide catalysts are still required.

Previously, many studies focused on the synthesis and characterization of various molybdenum polysulfido complexes and their precursors in the condensed phase, yielding diverse disulfide species [28-30, 32-35]. Among these, the $[\text{Mo}_2\text{S}_n]^{2-}$ anion was found to possess a terminal S_2^{2-} ligand [32], $[\text{Mo}_2\text{S}_n]^{2-}$ was considered

to have two terminal S² ligands [33], [Mo S]² was reported to contain four terminal S² and two bridging S² ligands [30], and [Mo S]² was predicted to have three bridging S² and three terminal S² ligands [29]. These molybdenum complexes containing persulfido (S²) ligands may lead to corresponding complexes with supersulfido (S³) ligands via further electron transfer, though less is known about their supersulfido complexes [36–40].

Gas-phase clusters serve as effective molecular models for gaining microscopic understanding of complex surface structures and catalytic processes at the molecular level [41–45]. Theoretical calculations play an indispensable role in describing the accurate structures and properties of gas-phase clusters [46]. Over the past few years, considerable efforts have been devoted to studying mono- and multi-nuclear molybdenum sulfide gas-phase clusters [47–60]. Andrews' s group investigated infrared spectra combined with DFT calculations of neutral mono-nuclear MS (M = Cr, Mo, W; n = 1–3) clusters [59]. Gemming et al. reported joint experimental photoelectron spectra and theoretical investigations on various mono- and multi-nuclear molybdenum sulfide clusters [53, 57, 58]. Jiao et al. presented the structure and reactivity of the Mo S cluster as a model for amorphous molybdenum sulfide MoS [54]. Murugan et al. reported an ab initio study on the structural stability of Mo-S clusters and size-specific stoichiometries of magic clusters [56], wherein Mo S consisting of two bridging S and three terminal S atoms was expected to be the magic cluster. Despite these efforts, systematic theoretical investigations on gas-phase molybdenum sulfide clusters are still needed.

In our previous work [61, 62], we reported a theoretical study on mono-nuclear molybdenum sulfide clusters, MoS / (n = 1–6). To mimic the geometric and electronic properties of molybdenum sulfide surfaces and defects, larger Mo S_n clusters are of interest. In the present work, extensive DFT and CCSD(T) calculations were performed to elucidate the structural and electronic properties of di-nuclear molybdenum sulfide clusters, Mo S₂ and Mo S_n (n = 4–8). This study continues our research interest in various clusters aimed at providing well-defined molecular models for bulk surfaces and catalysts [61–66].

According to our calculations, structural evolution behavior was found with the exception of neutral Mo S. The neutral Mo S can be viewed as replacing two terminal S atoms in Mo S_n with the same number of S units. Interestingly, diverse disulfur ligands, including supersulfido (S³) ligands, emerged in sulfur-rich clusters Mo S_n / (n = 7, 8). Disulfur species may have a key impact on catalytic activity [67–69]. Our calculations showed that reduction reactions for removing one sulfur atom from sulfur-rich clusters were spontaneous, whereas reactions were non-spontaneous when sulfur atoms were removed from sulfur-deficient clusters. These results suggest that S units may play an important role in removing sulfur atoms from edge sites of fresh MoS catalysts.

2. COMPUTATIONAL METHODS

The computational details for this study are similar to our earlier work on mononuclear molybdenum sulfide clusters, MoS_n ($n = 1-6$) [61, 62]. Density functional theory (DFT) calculations employing the B3LYP hybrid functional [70-72] were carried out using the Gaussian 03 program [73]. B3LYP is widely used in quantum chemistry [74] and has been applied to other Mo-S systems, showing good agreement with experimental data [51, 54, 59]. Additionally, B3LYP gave reasonably good results compared to available experimental data in our previous work [61-66]. As discussed below, we used B3LYP functional results for further discussion.

A host of initial structures considering different spin states and geometric symmetries were evaluated. The search for the most stable structures was first performed using the triple- valence plus polarization (def2-TZVP) basis set [75-77] and the corresponding Stuttgart effective core potential for Mo [78] (denoted as L-BS hereafter). Then selected low-lying isomers ($E < 0.50$ eV) were further re-optimized at the B3LYP level with larger basis sets: the Stuttgart relativistic small core basis set and effective core potential [78, 79] augmented with two f-type and one g-type polarization functions ($\alpha(f) = 0.338, 1.223$; $\alpha(g) = 0.744$) for molybdenum [80], and the aug-cc-pVTZ basis set for sulfur and hydrogen [81-83] (denoted as H-BS hereafter). Scalar relativistic effects were taken into account via quasi-relativistic pseudo-potentials.

Vibrational frequencies were calculated at the same level of theory to confirm that reported minima have no imaginary frequencies. The relative stabilities of several energetically close-lying isomers ($E < 0.40$ eV) were further distinguished with higher-level CCSD(T) [84-88] single-point calculations using H-BS basis sets at B3LYP optimized geometries. Vertical electron detachment energies (VDEs) were calculated based on the generalized Koopmans' theorem [89], which was described in detail in our previous studies [61-66].

All DFT calculations were performed using Gaussian 03 software. CCSD(T) calculations were performed with MOLPRO 2010.1 package [90]. Frontier molecular orbitals were visualized using VMD software [91].

3. THEORETICAL RESULTS

Optimized geometries for ground-state and selected energetically low-lying isomers of MoS_n and MoS_n ($n = 4-8$) at the B3LYP/H-BS level are displayed in Figs. 1-5. Their relative energies, including isomers within 0.40 eV at the B3LYP/H-BS level together with CCSD(T) single-point calculation results, are collected in Table 1. Alternative optimized results at the B3LYP/L-BS level for MoS_n ($n = 4-8$) are given in the Supporting Information (Figs. S1-S5).

3.1 Sulfur-deficient clusters: Mo S and Mo S (n = 4, 5)

Previously, tribridged structures with three bridging S atoms and dibridged structures with two bridging S atoms and one terminal S atom were reported as possible ground states of the Mo S cluster [56, 58]. To search for ground states of Mo S / , numerous initial structures were considered, including the aforementioned dibridged and tribridged structures.

Based on calculations, a nonplanar dibridged structure (C , ³A') is the lowest-energy structure of Mo S (Fig. 1a [Figure 1: see original paper]). Another triplet state (³A) with higher symmetry C is only 0.04 eV higher in energy (Fig. 1b). The corresponding quintet state (B) with C symmetry lies 0.15 eV higher (Fig. 1c). The quintet state (B_g) with C symmetry is 0.21 eV higher (Fig. 1d). The difference between these two quintet states is that two terminal S atoms in the former show a syn relationship, whereas the latter has an anti configuration. Additionally, the triplet state (C , ³A'') with anti configuration is 0.30 eV higher (Fig. 1e). The syn configuration appears more stable than the anti configuration. Previous studies [47, 48, 56, 58] also supported the dibridged structure with syn configuration as the ground state of Mo S .

For the anionic species, the dibridged structure (C , B) with syn configuration is the lowest-energy structure of Mo S (Fig. 1g). Two other dibridged isomers, C (B_g) and C (²B), lie 0.18 eV (Fig. 1h) and 0.34 eV (Fig. 1i) higher in energy, respectively. Other optimized isomers for both neutral and anionic species are much higher in energy and thus not listed. More optimized structures at the B3LYP/L-BS level are available in the Supporting Information (Fig. S1).

Starting from the ground states of Mo S / clusters, extensive structural searches revealed the singlet (C , ¹A') as the ground state of Mo S (Fig. 2a [Figure 2: see original paper]), which can be viewed as adding a terminal S atom to the dibridged Mo S . Previous studies by Murugan et al. [56] and Gemming et al. [58] support our results. The corresponding triplet state (C , ³A') is 0.17 eV higher (Fig. 2b). For anionic Mo S , the ground state (Fig. 2c) is a doublet state (C , ²A') with geometry similar to the neutral ground state. A quartet (C , A) lies 0.22 eV above the ground state (Fig. 2d).

3.2 Stoichiometric clusters: Mo S and Mo S

The ground state of Mo S has C (¹A) symmetry (Fig. 3a [Figure 3: see original paper]), which can be considered as adding a terminal S atom to the Mo S ground state. Each Mo atom in Mo S is tetra-coordinated with two terminal S atoms and two bridging S atoms. This result is consistent with the previous study by Gemming et al. [58]. It should be mentioned that Murugan et al. [56] expected the isomer with a terminal S unit to be the most stable structure of Mo S , but this isomer is less stable (>0.50 eV) than the structure in Fig. 3a according to our calculations (Fig. S3). For anionic Mo S , an open-shell (²A_g) structure with D symmetry is the ground state (Fig. 3b).

3.3 Sulfur-rich clusters: Mo S and Mo S (n = 7, 8)

To our knowledge, no other computational studies have reported gas-phase Mo S / and Mo S / clusters. Based on our calculations for Mo S / , various initial configurations with different spin multiplicities were studied to search for ground states of Mo S / .

As shown in Fig. 4a [Figure 4: see original paper], the lowest-energy structure of Mo S is predicted to be a closed-shell (1A) with C symmetry containing a bridging S unit. It can be regarded as replacing one bridging S atom in Mo S with a bridging S unit. The S-S bond length of the S unit in Mo S (Fig. 4a) is 2.086 Å. A triplet state (C , $^3A''$) with a terminal S unit (Fig. 4b) lies 0.26 eV above the ground state. However, this structure becomes the ground state of the Mo S anion (Fig. 4d), whereas the structure with a bridging S unit (Fig. 4e) is 0.39 eV higher in energy. The Mo S ground state can be seen as replacing one terminal S atom in Mo S with a terminal S unit. The terminal S ligand in Mo S (Fig. 4d) is attached in a side-on fashion, with an S-S bond length of 2.097 Å.

For Mo S / , several close-lying isomers were found near the lowest-energy structure. As shown in Fig. 5a [Figure 5: see original paper], the ground state of Mo S is a 3B state with C symmetry, which can be viewed as replacing two terminal S atoms in Mo S with two terminal S units in a syn configuration. The S-S bond lengths in the S units are calculated to be 1.999 Å, and the Mo-S bond lengths are 2.468 Å. Another triplet state (C , 3B_u) also has two terminal S ligands but in an anti configuration, lying 0.20 eV higher (Fig. 5b). The isomer formed by replacing the remaining bridging S in Mo S with a bridging S unit is much higher in energy (>0.5 eV; Fig. S5).

For the anion, the most stable structure of Mo S (Fig. 5c) is a doublet state with C symmetry, where two terminal S ligands are in a syn relationship as in the neutral case. The anti isomer (C , 2B_g) is 0.06 eV higher (Fig. 5d). Additionally, the isomer containing a terminal S ligand is 0.11 eV higher (Fig. 5e). Similar to Mo S / results, calculations show that the syn configuration appears more stable than the anti configuration for Mo S .

3.4 CCSD(T) single-point calculations for low-lying structures

Low-lying isomers of Mo S (n = 4-8) and their anionic species (within 0.40 eV at the B3LYP/H-BS level) were further evaluated using higher-level CCSD(T) single-point calculations at B3LYP geometries. Relative energies from CCSD(T) calculations are summarized in Table 1. Overall, CCSD(T) results are in good agreement with DFT/B3LYP calculations, except for neutral Mo S . According to CCSD(T) calculations (Table 1), the second lowest-energy isomer (C , 3A ; Fig. 1b) of Mo S appears more stable than the isomer (C , $^3A''$) shown in Fig. 1a. Although these two isomers are close in energy (0.07 eV) at the CCSD(T) level, they are similar in geometry and electronic structure. Herein, the Mo S (C , 3A) shown in Fig. 1b is tentatively considered the ground state.

4. DISCUSSION

4.1 Interpretation of simulated spectra and molecular orbital analyses

Experimental PES spectra serve as an electronic “fingerprint” of a given cluster, providing valuable electronic information. Based on the generalized Koopmans’ theorem, vertical detachment energies (VDEs) for identified Mo S_n (n = 4–8) anionic ground states and selected low-lying isomers (E < 0.40 eV) were calculated (Table 2). The principles of PES simulation are described in early references [92]. This method has been extensively used in previous studies [61, 66, 94–96] and shows good agreement with experimental spectra. Simulated PES spectra are presented in Fig. 12 [Figure 12: see original paper]. The first vertical detachment energy (VDE) trend as a function of S content (n) in Mo S_n (n = 4–8) is displayed in Fig. 13 [Figure 13: see original paper].

4.1.1 Mo S and Mo S Frontier orbitals of Mo S and Mo S are illustrated in Fig. 6 [Figure 6: see original paper]. As mentioned above, Mo S (C, ³A) shown in Fig. 1b is considered the ground state based on CCSD(T) single-point calculations. Its valence electronic configuration is (18a)²(10b)²(6a)¹(19a)¹. Addition of an electron into the empty antibonding orbital 13b of the neutral (Fig. 6a) leads to the anionic ground state Mo S (C, B) shown in Fig. 1g, with valence electronic configuration (10b)²(18a)²(6a)¹(13b)¹(19a)¹. Accordingly, Mo–Mo distances increase from 2.616 to 2.760 Å (Figs. 1b and 1g). The VDE upon photodetachment from the singly occupied bonding orbital (19a)¹, which is mainly characterized by a Mo 4d orbital, is predicted to be 3.39 eV. The fully occupied 10b MO and lower orbitals are primarily of S 3p character. Other calculated VDEs from 13b and below are presented in Table 2.

4.1.2 Mo S and Mo S The ground state of neutral Mo S (C, ¹A’) is predicted to be a closed-shell species (Fig. 2a). The valence electronic configuration of Mo S is (36a’)²(37a’)². Addition of an electron into the empty bonding orbital 38a’ of the neutral (Fig. 7a [Figure 7: see original paper]) leads to the anionic ground state Mo S (C, ²A’; Fig. 2c) with valence electronic configuration (36a’)²(37a’)²(38a’)¹. As shown in Fig. 7b, the singly occupied molecular orbital (SOMO) 38a’ and the fully occupied orbital 36a’ primarily correspond to Mo 4d orbitals, while orbital 37a’ is characterized by S 3p features. The first detachment channel for Mo S derives from removal of the SOMO 38a’, with a calculated VDE of 3.76 eV.

4.1.3 Mo S and Mo S Neutral Mo S (Fig. 3a) is stoichiometric, with each Mo achieving its highest oxidation state of Mo⁶⁺. In other words, all six valence electrons of Mo [4d⁵5s¹] are used to form bonds with S atoms. The valence electronic configuration of neutral Mo S (C, ¹A) is (24a)²(12b)²(19b)². The

highest occupied molecular orbital (HOMO) 19b and lowest unoccupied molecular orbital (LUMO) 25a are depicted in Fig. 8a [Figure 8: see original paper]. All MOs from HOMO downward are S 3p-based orbitals, and the LUMO is primarily featured by the Mo 4d orbital.

When one extra electron is added to neutral Mo S, the ground state of Mo S (Fig. 3b) maintains the neutral skeleton, though the rhombus Mo S unit is distorted relative to the anion. The valence electronic configuration of Mo S ($D_{2h}, ^2A_g$) is $(4b_g)^2(10b_u)^2(15a_g)^1$. In this D_{2h} structure, the extra electron is delocalized over the two Mo atoms, as evidenced by its SOMO 15a_g (Fig. 8b). Photodetachment from SOMO 15a_g yields VDE with a calculated value of 4.51 eV. Remaining calculated VDEs from 10b_u and below are presented in Table 2.

4.1.4 Mo S and Mo S For sulfur-rich Mo S, the structure with an S unit in bridging fashion is predicted to be the neutral ground state (Fig. 4a), with valence electronic configuration $(35a)^2(33b)^2(36a)^2(34b)^2$. All MOs feature S 3p orbitals (Fig. 9a [Figure 9: see original paper]). The anion Mo S ($C_{2v}, ^2A$) ground state is predicted to be open-shell with a terminal S group (Fig. 4d). The valence electronic configuration is $(65a)^2(66a)^2(67a)^2(68a)^1(69a)^2(70a)^2(71a)^2$. The calculated S-S bond length in this S group is 2.097 Å, similar to free S²⁻ ($^1\Sigma_g^-$) dianion (2.180 Å calculated at the same level). The two fully occupied orbitals 71a and 65a correspond to σ^* orbitals of the S group (Fig. 9b). Hence, Mo S ($C_{2v}, ^1A$) can be considered as addition of an S²⁻ unit to the cationic Mo S. Photodetachment from the fully occupied orbital 71a yields the first PES band with calculated VDEs of 4.32 eV () and 4.26 eV (). Detachment originating from the singly occupied orbital 68a requires higher energy (5.00 eV).

4.1.5 Mo S and Mo S Frontier MOs of Mo S and Mo S are illustrated in Fig. 10 [Figure 10: see original paper]. The Mo S ground state is 3B_1 with C_{2v} symmetry (Fig. 5a). The valence electronic configuration for the neutral species is $(16b)^2(26a)^2(17b)^1(13a)^1(18b)^2(27a)^2$. Corresponding frontier MO pictures are shown in Fig. 10a, where two singly occupied orbitals 13a, 17b and two doubly occupied orbitals 16b and 18b correspond to σ^* orbitals of two bound S units in Mo S ($C_{2v}, ^3B_1$). Furthermore, the S-S bond length of the S moiety (1.999 Å in Fig. 5a) is very close to that of free S²⁻ ($^2\Pi_g^-$) anion (2.029 Å calculated at the same level). Spin density analyses further confirm that two unpaired electrons are separately located on two S units (Fig. 11a [Figure 11: see original paper]). Therefore, Mo S ($C_{2v}, ^3B_1$) may be viewed as two S units adhered to the cationic Mo S²⁺.

For the anionic species, the valence electronic configuration is $(16b)^2(26a)^2(17b)^2(27a)^2(13a)^2(18b)^1$. As shown in Fig. 10b, the singly occupied MO 18b and three doubly occupied MOs 13a, 17b, and 16b correspond to σ^* orbitals of the S-S moieties. The S unit bond length (2.055 Å) is between those of bound S and S²⁻ anions (1.999 Å in Fig. 5a and 2.097 Å in Fig. 4d, respectively). Spin density analyses show

that an unpaired electron is equiprobably shared by two terminal S groups (Fig. 11b). Therefore, the Mo S (C, ²B; Fig. 5c) cluster can be described as a resonance hybrid of two equivalent C structures with both S and S² units. As shown in Table 2 and Fig. 12e, photodetachment from the fully occupied 13a orbital (Fig. 10b) of Mo S yields the first PES band with calculated VDE of 3.58 eV ().

4.2 Structural evolution of Mo S / (n = 4-8) clusters

As noted above, a series of thiomolybdate dianions Mo S²⁻ (n = 6-9) have been prepared and characterized in the condensed phase [33]. It was pointed out that six homologues [Mo S]²⁻ (n = 6-12) may be interconverted by adding sulfur or removing sulfur with triphenylphosphine (Ph₃P) [32]. Our paper finds similar structural evolutions for gas-phase Mo S / (n = 4-8) clusters.

It is worth mentioning that Gemming et al. [58] showed Mo S has the highest stability among Mo S_y clusters, suggesting its structure may serve as a motif for larger Mo S_y clusters or bulk MoS phase. In our calculations, the ground state of Mo S (C, ¹A; Fig. 3a) possesses four Mo=S double bonds and four Mo-S single bonds, with each Mo atom at its highest oxidation state of +6.

For neutral clusters, as sulfur content increases, the formal oxidation state of molybdenum increases until reaching +6. Meanwhile, sulfur atoms successively occupy terminal sites in Mo S clusters (n = 4-6). After both Mo atoms reach the highest oxidation state, disulfur units (S₂) begin to emerge: one bridging S atom in Mo S is replaced by a bridging S unit in Mo S, and two terminal S atoms in Mo S are replaced by terminal S ligands in Mo S.

Similar evolutionary patterns are found for anionic Mo S⁻ (n = 4-6) clusters, which preserve the structural skeleton of their neutral counterparts. In Mo S⁻, one terminal S atom in Mo S is replaced by a terminal S ligand. Subsequently, in Mo S⁻, two terminal S atoms in Mo S are replaced by terminal S ligands. Furthermore, based on relative stabilities of Mo S and Mo S / (Figs. 1 and 5), the syn configuration appears more stable than the anti configuration.

4.3 Trend of VDE as a function of S content in Mo S (n = 4-8)

Fig. 13 depicts the calculated VDE trend as a function of S content in Mo S clusters. This trend can be qualitatively understood from frontier MO analysis (Figs. 6-10). VDE increases nearly linearly with sulfur content (n = 4-6), clearly showing sequential sulfidation behavior of the Mo dimer. Valence electrons of molybdenum (4d⁵5s¹) are sequentially transferred to added S atoms, accompanied by decreasing numbers of Mo 4d-based orbitals (Figs. 6-8).

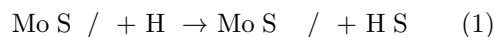
Interestingly, VDE suddenly begins to decrease thereafter. This decrease can be understood from frontier MO analysis (Figs. 9 and 10). When n reaches 7 (Mo S), detachment originates from fully occupied * orbitals (71a) of an S unit, causing VDE to decrease (from 4.51 to 4.26 eV). When n equals eight

(Mo S_n), VDE corresponds to detachment from singly occupied * orbitals (18b) of two S moieties. The further decrease in VDE from 4.26 to 3.58 eV may result from distribution of an unpaired electron over * orbitals of two S groups.

4.4 Reduction reaction of H₂ on Mo S_n / (n = 4-8) clusters

Afanasiev et al. [67, 68] showed that S² species located at edges of fresh MoS catalysts play a key role in catalytic activity. Recently, Karunadasa and co-workers [28] reported synthesis of a side-on bound Mo₂-disulfide complex that could mimic MoS edge sites for catalytic hydrogen generation. Diverse S units are found in sulfur-rich clusters Mo S_n / (n = 7, 8) in our work.

MoS catalysts are typically used in H₂/H₂S gaseous environments at elevated temperatures. Experiments indicated that kinetics of S group interaction with hydrogen could be promoted by reactant H₂ and hindered by product H₂S [67]. Thus, we propose reaction (eq. 1) removing a sulfur atom from Mo S_n / (n = 4-8) clusters. The driving force can be estimated by negative values of Gibbs free energy differences (ΔG), obtained via equation (eq. 2) and summarized in Table 3.



$$\Delta G = G(\text{Mo S}_{n-1} /) + G(\text{H}_2\text{S}) - G(\text{Mo S}_n /) - G(\text{H}_2) \quad (2)$$

Based on ΔG values, driving forces for the proposed reactions increase with n. For reactions (Eq. 1; n = 5, 6), sulfur is removed from terminal S of Mo S_n / and Mo S_n. Corresponding ΔG values (Table 3) are positive (reactant-favored). After both Mo atoms reach maximum oxidation state +6, S units begin to emerge. Energy costs (ΔG) for losing sulfur atoms from various S units become negative (product-favored). Therefore, for sulfur-rich clusters Mo S_n / (n = 7, 8), the proposed reactions (Eq. 2) may be energetically (thermodynamically) favored regardless of kinetic factors.

In neutral Mo S_n, a bridging disulfide (S²) ligand appears. The Gibbs free energy difference (ΔG) is predicted to be -0.94 kcal · mol⁻¹, corresponding to removal of an S atom from the bridging disulfide S² moiety in Mo S_n. For its anion and Mo S_n⁻, S atoms are removed from terminal S² and terminal S units in the reaction (Eq. 1; n = 7, 8), respectively. Corresponding ΔG values are estimated to be -12.51 kcal · mol⁻¹ (S² for Mo S_n) and -14.74 kcal · mol⁻¹ (S for Mo S_n). Generally, driving forces (- ΔG) for removing a sulfur atom from various S ligands in Mo S_n / (n = 4-8) clusters follow the order: t-S² < b-S² < t-S² < t-S, representing terminal S atom, bridging (-¹:¹) S², terminal (²) S², and terminal (²) S units, respectively. S units appear more reactive with H₂, which removes an S atom via H₂S release. Coordination unsaturated sites (CUS) can be obtained by removing sulfur atoms from MoS catalyst edges under H₂ atmosphere [67]. This order may provide insight into pretreatment of fresh MoS catalysts under hydrogen conditions.

5. CONCLUSION

We report a systematic theoretical study on dinuclear metal sulfide clusters: Mo_nS_m and Mo_nS ($n = 4-8$). DFT and CCSD(T) calculations were carried out to elucidate chemical bonding, geometric, and electronic properties of Mo_nS_m clusters. Calculations showed that sulfur atoms tend to occupy terminal sites continuously during sequential sulfidation. After Mo atoms reach maximum oxidation state +6, diverse disulfur ligands emerge in sulfur-rich Mo_nS_m ($n = 7, 8$) clusters.

By calculating free energy differences (ΔG) for reaction (eq. 1), we found ΔG values were positive for sulfur-deficient and stoichiometric clusters (eq. 2; $n = 5, 6$) but negative for sulfur-rich species (Eq. 2; $n = 7, 8$). Driving forces ($-\Delta G$) for reactions eliminating sulfur from diverse S ligands in Mo_nS_m ($n = 4-8$) clusters follow the general order: $\text{t-S} < \text{b-S}^2 < \text{t-S}^2 < \text{t-S}$. This order may provide insight into pretreatment of fresh MoS catalysts under H_2 atmosphere.

REFERENCES

- (1) Rapoport, L.; Moshkovich, A.; Perfilyev, V.; Laikhtman, A.; Lapsker, I.; Yadgarov, L.; Rosentsveig, R.; Tenne, R. High lubricity of Re-doped fullerene-like MoS nanoparticles. *Tribol. Lett.* **2012**, *45*, 257-264.
- (2) Ye, L. N.; Wu, C. Z.; Guo, W.; Xie, Y. MoS hierarchical hollow cubic cages assembled by bilayers: one-step synthesis and electrochemical hydrogen storage properties. *Chem. Commun.* **2006**, *45*, 4738-4740.
- (3) Walter, M. G.; Warren, E. L.; McKone, J. R.; Boettcher, S. W.; Mi, Q. X.; Santori, E. A.; Lewis, N. S. Solar water splitting cells. *Chem. Rev.* **2010**, *110*, 6446-6473.
- (4) Kisielowski, C.; Ramasse, Q. M.; Hansen, L. P.; Brorson, M.; Carlsson, A.; Molenbroek, A. M.; Topsøe, H.; Helveg, S. Imaging MoS nanocatalysts with single-atom sensitivity. *Angew. Chem. Int. Ed.* **2010**, *49*, 2708-2710.
- (5) Jaramillo, T. F.; Jørgensen, K. P.; Bonde, J.; Nielsen, J. H.; Horch, S.; Chorkendorff, I. Identification of active edge sites for electrochemical H_2 evolution from MoS nanocatalysts. *Science* **2007**, *317*, 100-102.
- (6) Vajda, S.; White, M. G. Catalysis applications of size-selected cluster deposition. *ACS Catal.* **2015**, *5*, 7152-7176.

- (7) Deng, Y.; Ting, L. R. L.; Neo, P. H. L.; Zhang, Y. J.; Peterson, A. A.; Yeo, B. S. Operando Raman spectroscopy of amorphous molybdenum sulfide (MoS₂) during electrochemical hydrogen evolution: identification of sulfur atoms as catalytically active sites for H₂ reduction. *ACS Catal.* **2016**, *6*, 7790–7798.
- (8) Truong, Q. D.; Devaraju, M. K.; Nguyen, D. N.; Gambe, Y.; Nayuki, K.; Sasaki, Y.; Tran, P. D.; Honma, I. Disulfide-bridged (MoS₂)_n cluster polymer: molecular dynamics and application as electrode material for rechargeable magnesium battery. *Nano Lett.* **2016**, *16*, 5829–5835.
- (9) Kokko, M.; Bayerköhler, F.; Erben, J.; Zengerle, R.; Kurz, P.; Kerzenmacher, S. Molybdenum sulphides on carbon supports as electrocatalysts for hydrogen evolution in acidic industrial wastewater. *Appl. Energ.* **2017**, *190*, 1221–1233.
- (10) Seger, B.; Herbst, K.; Pedersen, T.; Abrams, B.; Vesborg, P. C. K.; Hansen, O.; Chorkendorff, I. MoS₂ clusters as effective H₂ evolution catalyst on protected Si photocathodes. *J. Electrochem. Soc.* **2014**, *161*, H722–H724.
- (11) Vrabel, H.; Merki, D.; Hu, X. Hydrogen evolution catalyzed by MoS₂ and MoS₃ particles. *Energy Environ. Sci.* **2012**, *5*, 6136–6144.
- (12) Lau, V. W. H.; Masters, A. F.; Bond, A. M.; Maschmeyer, T. Ionic-liquid-mediated active-site control of MoS₂ for electrocatalytic hydrogen evolution. *Chem. Eur. J.* **2012**, *18*, 8230–8239.
- (13) Guo, X. N.; Tong, X. L.; Wang, Y. W.; Chen, C. M.; Jin, G. Q.; Guo, X. Y. High photoelectrocatalytic performance of MoS₂-SiC hybrid structure for hydrogen evolution. *J. Mater. Chem. A* **2013**, *1*, 4657–4661.
- (14) Liao, L.; Zhu, J.; Bian, X. J.; Zhu, L. N.; Scanlon, M. D.; Girault, H. H.; Liu, B. H. MoS₂ formed on mesoporous graphene as highly active catalyst for hydrogen evolution. *Adv. Funct. Mater.* **2013**, *23*, 5326–5333.
- (15) Gary, J. H.; Handwerk, G. E.; Kaiser, M. J. *Petroleum Refining: Technology and Economics*, 5th Edition; CRC Press: Boca Raton, Florida, 2007.
- (16) Liu, D.; Li, Z.; Sun, Q.; Kong, X.; Zhao, A. Z.; Wang, Z. X. In situ FT-IR study of thiophene adsorbed on sulfided Mo catalysts. *Fuel* **2012**, *92*, 77–83.
- (17) Ramos, M.; Berhault, G.; Ferrer, D. A.; Torres, B.; Chianelli, R. R. HRTEM and molecular modeling of MoS₂-CoS interface: understanding promotion in bulk HDS catalysts. *Catal. Sci. Technol.* **2012**, *2*, 164–

178.

- (18) Vogelaar, B. M.; Kagami, N.; van der Zijden, T. F.; van Langeveld, A. D.; Eijsbouts, S.; Moulijn, J. A. Relation between sulfur coordination of active sites and HDS activity for Mo and NiMo catalysts. *J. Mol. Catal. A: Chem.* **2009**, *309*, 79–88.
- (19) Lauritsen, J. V.; Bollinger, M. V.; Lægsgaard, E.; Jacobsen, K. W.; Nørskov, J. K.; Clausen, B. S.; Topsøe, H.; Besenbacher, F. Atomic-scale insight into structure and morphology changes of MoS₂ nanoclusters in hydrotreating catalysts. *J. Catal.* **2004**, *221*, 510–522.
- (20) Topsøe, H.; Hinnemann, B.; Nørskov, J. K.; Lauritsen, J. V.; Besenbacher, F.; Hansen, P. L.; Hytoft, G.; Egeberg, R. G.; Knudsen, K. G. Role of reaction pathways and support interactions in development of high activity hydrotreating catalysts. *Catal. Today* **2005**, *107-108*, 12–22.
- (21) Vogelaar, B. M.; Steiner, P.; van der Zijden, T. F.; van Langeveld, A. D.; Eijsbouts, S.; Moulijn, J. A. Catalyst deactivation during thiophene HDS: role of structural sulfur. *Appl. Catal. A: Gen.* **2007**, *318*, 28–36.
- (22) Besenbacher, F.; Brorson, M.; Clausen, B. S.; Helveg, S.; Hinnemann, B.; Kibsgaard, J.; Lauritsen, J. V.; Moses, P. G.; Nørskov, J. K.; Topsøe, H. Recent STM, DFT and HAADF-STEM studies of sulfide-based hydrotreating catalysts: insight into mechanistic, structural and particle size effects. *Catal. Today* **2008**, *130*, 86–96.
- (23) Moses, P. G.; Hinnemann, B.; Topsøe, H.; Nørskov, J. K. Effect of copromotion on MoS₂ catalysts for hydrodesulfurization of thiophene: density functional study. *J. Catal.* **2009**, *268*, 201–208.
- (24) Joshi, Y. V.; Ghosh, P.; Venkataraman, P. S.; Delgass, W. N.; Thomson, K. T. Electronic descriptors for adsorption energies of sulfur-containing molecules on Co/MoS₂ using DFT calculations. *J. Phys. Chem. C* **2009**, *113*, 9698–9709.
- (25) Joshi, Y. V.; Ghosh, P.; Daage, M.; Delgass, W. N. Support effects in HDS catalysts: DFT analysis of thiolysis and hydrolysis energies of metal-support linkages. *J. Catal.* **2008**, *257*, 71–80.
- (26) Travert, A.; Nakamura, H.; van Santen, R. A.; Cristol, S.; Paul, J. F.; Payen, E. Hydrogen activation on Mo-based sulfide catalysts, periodic DFT study. *J. Am. Chem. Soc.* **2002**, *124*, 7084–7095.
- (27) Topsøe, H.; Clausen, B. S.; Massoth, F. E. Hydrotreating Catalysis in *Catalysis-Science and Technology*; Anderson, J. R.; Boudart, M., Eds.;

1st Edition; Springer-Verlag Berlin Heidelberg: New York, 1996.

- (28) Karunadasa, H. I.; Montalvo, E.; Sun, Y. J.; Majda, M.; Long, J. R.; Chang, C. J. Molecular MoS edge site mimic for catalytic hydrogen generation. *Science* **2012**, *335*, 698–702.
- (29) Kibsgaard, J.; Jaramillo, T. F.; Besenbacher, F. Building appropriate active-site motif into hydrogen-evolution catalyst with thiomolybdate [Mo S]² clusters. *Nat. Chem.* **2014**, *6*, 248–253.
- (30) Huang, Z. J.; Luo, W. J.; Ma, L.; Yu, M. Z.; Ren, X. D.; He, M. F.; Polen, S.; Click, K.; Garrett, B.; Lu, J.; Amine, K.; Hadad, C.; Chen, W. L.; Asthagiri, A.; Wu, Y. Y. Dimeric [Mo S]² cluster: molecular analogue of MoS edges for superior hydrogen-evolution electrocatalysis. *Angew. Chem. Int. Ed.* **2015**, *54*, 15181–15185.
- (31) Garrett, B. R.; Polen, S. M.; Click, K. A.; He, M.; Huang, Z.; Hadad, C. M.; Wu, Y. Tunable molecular MoS edge-site mimics for catalytic hydrogen production. *Inorg. Chem.* **2016**, *55*, 3960–3966.
- (32) Hadjikyriacou, A. I.; Coucouvanis, D. New members of [Mo (S) (S)]² series—synthesis, structural characterization, and properties of [Mo S]², [Mo S]², and [Mo S]² thio anions. *Inorg. Chem.* **1987**, *26*, 2400–2408.
- (33) Pan, W. H.; Harmer, M. A.; Halbert, T. R.; Stiefel, E. I. Induced internal redox processes in molybdenum-sulfur chemistry: conversion of MoS² to Mo S² by organic disulfides. *J. Am. Chem. Soc.* **1984**, *106*, 459–460.
- (34) Clegg, W.; Christou, G.; Garner, C. D.; Sheldrick, G. M. [Mo S]², complex with terminal sulfido, bridging sulfido, persulfido, and tetrasulfido groups. *Inorg. Chem.* **1981**, *20*, 1562–1566.
- (35) Pan, W. H.; Leonowicz, M. E.; Stiefel, E. I. Facile syntheses of new molybdenum and tungsten sulfido complexes. Structure of Mo S². *Inorg. Chem.* **1983**, *22*, 672–678.
- (36) Elder, R. C.; Trkula, M. Crystal structure of [(NH) RuSSRu(NH)]Cl · 2H O. Structural trans effect and evidence for supersulfide S bridge. *Inorg. Chem.* **1977**, *16*, 1048–1051.
- (37) York, J. T.; Brown, E. C.; Tolman, W. B. Characterization of complex comprising {Cu (S) }² core: bis(-S²)dicopper(III) or bis(-S ·)dicopper(II)? *Angew. Chem. Int. Ed.* **2005**, *44*, 7745–7748.
- (38) Yao, S.; Milsman, C.; Bill, E.; Wieghardt, K.; Driess, M. From paramagnetic mononuclear supersulfidonickel(II) complex to diamagnetic dimer

- with four-sulfur two-electron bond. *J. Am. Chem. Soc.* **2008**, *130*, 13536-13537.
- (39) Yao, S.; Xiong, Y.; Zhang, X.; Schlangen, M.; Schwarz, H.; Milsmann, C.; Driess, M. Facile dissociation of $[(\text{LNi})_n\text{E}]$ dichalcogenides: evidence for $[(\text{LNi})_n\text{E}]$ superselenides and supertellurides in solution. *Angew. Chem. Int. Ed.* **2009**, *48*, 4551-4554.
- (40) Camp, C.; Antunes, M. A.; García, G.; Ciofini, I.; Santos, I. C.; Pécaut, J.; Almeida, M.; Marçalo, J.; Mazzanti, M. Two-electron versus one-electron reduction of chalcogens by uranium(III): synthesis of terminal U(V) persulfide complex. *Chem. Sci.* **2014**, *5*, 841-846.
- (41) Johnson, G. E.; Tyo, E. C.; Castleman, A. W. Jr. Cluster reactivity experiments: employing mass spectrometry to investigate molecular-level details of catalytic oxidation reactions. *Proc. Natl. Acad. Sci. USA* **2008**, *105*, 18108-18113.
- (42) Waters, T.; Huang, X.; Wang, X. B.; Woo, H. K.; O' Hair, R. A. J.; Wedd, A. G.; Wang, L. S. Photoelectron spectroscopy of free multiply charged Keggin anions $[\text{PM}_n\text{O}]^3$ ($M = \text{Mo}, \text{W}$) in gas phase. *J. Phys. Chem. A* **2006**, *110*, 10737-10741.
- (43) Böhme, D. K.; Schwarz, H. Gas-phase catalysis by atomic and cluster metal ions: ultimate single-site catalysts. *Angew. Chem. Int. Ed.* **2005**, *44*, 2336-2354.
- (44) Castleman, A. W. Jr. Cluster structure and reactions: gaining insights into catalytic processes. *Catal. Lett.* **2011**, *141*, 1243-1253.
- (45) Kumar, C. A.; Saha, A.; Raghavachari, K. Bond activation and hydrogen evolution from water through reactions with M_nS ($M = \text{Mo}, \text{W}$) and W_nS anionic clusters. *J. Phys. Chem. A* **2017**, *121*, 1760-1767.
- (46) Castleman, A. W. Jr.; Jena, P. Clusters: bridge between disciplines. *Proc. Natl. Acad. Sci. USA* **2006**, *103*, 10552-10553.
- (47) Murugan, P.; Kumar, V.; Kawazoe, Y.; Ota, N. Atomic structures and magnetism in small MoS_n and WS_n clusters. *Phys. Rev. A* **2005**, *71*, 063203.
- (48) Murugan, P.; Kumar, V.; Kawazoe, Y.; Ota, N. Bonding nature and magnetism in small MoX_n ($X = \text{O}$ and S) clusters—comparative study by first principles calculations. *Chem. Phys. Lett.* **2006**, *423*, 202-207.
- (49) Patterson, M. J.; Lightstone, J. M.; White, M. G. Structure of molyb-

- denum and tungsten sulfide MS_y clusters: experiment and DFT calculations. *J. Phys. Chem. A* **2008**, *112*, 12011-12021.
- (50) Zhou, J.; Zhou, J.; Camillone, N.; White, M. G. Electronic charging of non-metallic clusters: size-selected MoS_y clusters supported on ultrathin alumina film on NiAl(110). *Phys. Chem. Chem. Phys.* **2012**, *14*, 8105-8110.
- (51) Bertram, N.; Kim, Y. D.; Ganteför, G.; Sun, Q.; Jena, P.; Tamuliene, J.; Seifert, G. Experimental and theoretical studies on inorganic magic clusters: MX ($M = W, Mo, X = O, S$). *Chem. Phys. Lett.* **2004**, *396*, 341-345.
- (52) Llusar, R.; Polo, V.; Velez, E.; Vicent, C. Sulfur-based redox reactions in MoS and MoS clusters bearing halide and 1,2-dithiolene ligands: mass spectrometric and density functional theory study. *Inorg. Chem.* **2010**, *49*, 8045-8055.
- (53) Gemming, S.; Seifert, G.; Götz, M.; Fischer, T.; Ganteför, G. Transition metal sulfide clusters below cluster-platelet transition: theory and experiment. *Phys. Status Solidi B* **2010**, *247*, 1069-1076.
- (54) Jiao, H. J.; Li, Y. W.; Delmon, B.; Halet, J. F. Structure and possible catalytic sites of MoS as model of amorphous molybdenum trisulfide: computational study. *J. Am. Chem. Soc.* **2001**, *123*, 7334-7339.
- (55) Mayhall, N. J.; Becher, E. L. III.; Chowdhury, A.; Raghavachari, K. Molybdenum oxides versus molybdenum sulfides: geometric and electronic structures of MoX_y ($X = O, S$ and $y = 6, 9$) clusters. *J. Phys. Chem. A* **2011**, *115*, 2291-2296.
- (56) Murugan, P.; Kumar, V.; Kawazoe, Y.; Ota, N. Ab initio study of structural stability of Mo-S clusters and size-specific stoichiometries of magic clusters. *J. Phys. Chem. A* **2007**, *111*, 2778-2782.
- (57) Gemming, S.; Seifert, G.; Bertram, N.; Fischer, T.; Götz, M.; Ganteför, G. One-dimensional (MoS) clusters: building blocks of cluster materials and ideal nanowires for molecular electronics. *Chem. Phys. Lett.* **2009**, *474*, 127-131.
- (58) Gemming, S.; Tamuliene, J.; Seifert, G.; Bertram, N.; Kim, Y. D.; Ganteför, G. Electronic and geometric structures of MoS_y and WS_y ($x = 1, 2, 4; y = 1-12$) clusters. *Appl. Phys. A* **2006**, *82*, 161-166.
- (59) Liang, B. Y.; Andrews, L. Infrared spectra and density functional theory calculations of group 6 transition metal sulfides in solid argon. *J. Phys.*

Chem. A **2002**, *106*, 6945-6951.

- (60) Pietsch, S.; Dollinger, A.; Strobel, C. H.; Park, E. J.; Gantefor, G.; Seo, H. O.; Kim, Y. D.; Idrobo, J. C.; Pennycook, S. J. Quest for inorganic fullerenes. *J. Appl. Phys.* **2015**, *118*, 134302.
- (61) Wang, B.; Wu, N.; Zhang, X. B.; Huang, X.; Zhang, Y. F.; Chen, W. K.; Ding, K. N. Probing smallest molecular model of MoS catalyst: S units in MoS / (n = 1-5) clusters. *J. Phys. Chem. A* **2013**, *117*, 5632-5641.
- (62) Wu, N.; Zhang, C. F.; Zhou, Q.; Huang, X.; Zhang, Y. F.; Ding, K. N.; Wang, B. DFT study on electronic and structural properties of MoS clusters. *Chin. J. Struc. Chem.* **2013**, *32*, 1046-1054.
- (63) Wang, B.; Chen, W. J.; Zhao, B. C.; Zhang, Y. F.; Huang, X. Tetratingsten oxide clusters $W O_n$ / (n = 10-13): structural evolution and chemical bonding. *J. Phys. Chem. A* **2010**, *114*, 1964-1972.
- (64) Zhai, H. J.; Wang, B.; Huang, X.; Wang, L. S. Probing electronic and structural properties of niobium trimer cluster and its mono- and dioxides: $Nb O_n$ and $Nb O_n$ (n = 0-2). *J. Phys. Chem. A* **2009**, *113*, 3866-3875.
- (65) Zhai, H. J.; Wang, B.; Huang, X.; Wang, L. S. Structural evolution, sequential oxidation, and chemical bonding in tritantalum oxide clusters: $Ta O_n$ and $Ta O_n$ (n = 1-8). *J. Phys. Chem. A* **2009**, *113*, 9804-9813.
- (66) Wang, B.; Zhai, H. J.; Huang, X.; Wang, L. S. On electronic structure and chemical bonding in tantalum trimer cluster. *J. Phys. Chem. A* **2008**, *112*, 10962-10967.
- (67) Afanasiev, P. Influence of reducing and sulfiding conditions on properties of unsupported MoS -based catalysts. *J. Catal.* **2010**, *269*, 269-280.
- (68) Afanasiev, P.; Jobic, H.; Lorentz, C.; Leverd, P.; Mastubayashi, N.; Piccolo, L.; Vrinat, M. Low-temperature hydrogen interaction with amorphous molybdenum sulfides MoS . *J. Phys. Chem. C* **2009**, *113*, 4139-4146.
- (69) Duchet, J.; Van Oers, E.; De Beer, V.; Prins, R. Carbon-supported sulfide catalysts. *J. Catal.* **1983**, *80*, 386-402.
- (70) Becke, A. D. New mixing of Hartree-Fock and local density-functional theories. *J. Chem. Phys.* **1993**, *98*, 1372-1377.
- (71) Lee, C.; Yang, W.; Parr, R. G. Development of Colle-Salvetti correlation-

- energy formula into functional of electron density. *Phys. Rev. B* **1988**, *37*, 785-789.
- (72) Stephens, P. J.; Devlin, F. J.; Chabalowski, C. F.; Frisch, M. J. Ab initio calculation of vibrational absorption and circular dichroism spectra using density functional force fields. *J. Phys. Chem.* **1994**, *98*, 11623-11627.
- (73) Frisch, M. J.; Trucks, G. W.; Schlegel, H. B.; Scuseria, G. E.; Robb, M. A.; Cheeseman, J. R.; Montgomery, J. A. Jr.; Vreven, T.; Kudin, K. N.; Burant, J. C.; Millam, J. M.; Iyengar, S. S.; Tomasi, J.; Barone, V.; Mennucci, B.; Cossi, M.; Scalmani, G.; Rega, N.; Petersson, G. A.; Nakatsuji, H.; Hada, M.; Ehara, M.; Toyota, K.; Fukuda, R.; Hasegawa, J.; Ishida, M.; Nakajima, T.; Honda, Y.; Kitao, O.; Nakai, H.; Klene, M.; Li, X.; Knox, J. E.; Hratchian, H. P.; Cross, J. B.; Bakken, V.; Adamo, C.; Jaramillo, J.; Gomperts, R.; Stratmann, R. E.; Yazyev, O.; Austin, A. J.; Cammi, R.; Pomelli, C.; Ochterski, J. W.; Ayala, P. Y.; Morokuma, K.; Voth, G. A.; Salvador, P.; Dannenberg, J. J.; Zakrzewski, V. G.; Dapprich, S.; Daniels, A. D.; Strain, M. C.; Farkas, O.; Malick, D. K.; Rabuck, A. D.; Raghavachari, K.; Foresman, J. B.; Ortiz, J. V.; Cui, Q.; Baboul, A. G.; Clifford, S.; Cioslowski, J.; Stefanov, B. B.; Liu, G.; Liashenko, A.; Piskorz, P.; Komaromi, I.; Martin, R. L.; Fox, D. J.; Keith, T.; Al-Laham, M. A.; Peng, C. Y.; Nanayakkara, A.; Challacombe, M.; Gill, P. M. W.; Johnson, B.; Chen, W.; Wong, M. W.; Gonzalez, C.; Pople, J. A. *Gaussian 03*, Revision D.01; Gaussian, Inc.: Wallingford, CT, 2004.
- (74) Sousa, S. F.; Fernandes, P. A.; Ramos, M. J. General performance of density functionals. *J. Phys. Chem. A* **2007**, *111*, 10439-10452.
- (75) Schäfer, A.; Huber, C.; Ahlrichs, R. Fully optimized contracted Gaussian basis sets of triple zeta valence quality for atoms Li to Kr. *J. Chem. Phys.* **1994**, *100*, 5829-5835.
- (76) Weigend, F.; Ahlrichs, R. Balanced basis sets of split valence, triple zeta valence and quadruple zeta valence quality for H to Rn: design and assessment of accuracy. *Phys. Chem. Chem. Phys.* **2005**, *7*, 3297-3305.
- (77) Eichkorn, K.; Weigend, F.; Treutler, O.; Ahlrichs, R. Auxiliary basis sets for main row atoms and transition metals and their use to approximate Coulomb potentials. *Theor. Chem. Acc.* **1997**, *97*, 119-124.
- (78) Andrae, D.; Haeussermann, U.; Dolg, M.; Stoll, H.; Preuss, H. Energy-adjusted ab initio pseudopotentials for second and third row transition elements. *Theor. Chim. Acta* **1990**, *77*, 123-141.
- (79) Küchle, W.; Dolg, M.; Stoll, H.; Preuss, H. Pseudopotentials

of the Stuttgart/Dresden Group, 1998, revision August 11, 1998; <http://www.theochem.uni-stuttgart.de/pseudopotentiale>.

- (80) Martin, J. M. L.; Sundermann, A. Correlation consistent valence basis sets for use with Stuttgart-Dresden-Bonn relativistic effective core potentials: atoms Ga-Kr and In-Xe. *J. Chem. Phys.* **2001**, *114*, 3408-3420.
- (81) Dunning, T. H. Jr. Gaussian basis sets for use in correlated molecular calculations. I. Atoms boron through neon and hydrogen. *J. Chem. Phys.* **1989**, *90*, 1007-1023.
- (82) Woon, D. E.; Dunning, T. H. Jr. Gaussian basis sets for use in correlated molecular calculations. III. Atoms aluminum through argon. *J. Chem. Phys.* **1993**, *98*, 1358-1371.
- (83) Dunning, T. H.; Peterson, K. A.; Wilson, A. K. Gaussian basis sets for use in correlated molecular calculations. X. Atoms aluminum through argon revisited. *J. Chem. Phys.* **2001**, *114*, 9244-9253.
- (84) Purvis, G. D. III; Bartlett, R. J. Full coupled-cluster singles and doubles model: inclusion of disconnected triples. *J. Chem. Phys.* **1982**, *76*, 1910-1918.
- (85) Scuseria, G. E.; Janssen, C. L.; Schaefer, H. F. III. Efficient reformulation of closed-shell coupled cluster single and double excitation (CCSD) equations. *J. Chem. Phys.* **1988**, *89*, 7382-7387.
- (86) Raghavachari, K.; Trucks, G. W.; Pople, J. A.; Head-Gordon, M. 5th-order perturbation comparison of electron correlation theories. *Chem. Phys. Lett.* **1989**, *157*, 479-483.
- (87) Watts, J. D.; Gauss, J.; Bartlett, R. J. Coupled-cluster methods with noniterative triple excitations for restricted open-shell Hartree-Fock and other general single determinant reference functions—energies and analytical gradients. *J. Chem. Phys.* **1993**, *98*, 8718-8733.
- (88) Bartlett, R. J.; Musial, M. Coupled-cluster theory in quantum chemistry. *Rev. Mod. Phys.* **2007**, *79*, 291-352.
- (89) Tozer, D. J.; Handy, N. C. Improving virtual Kohn-Sham orbitals and eigenvalues: application to excitation energies and static polarizabilities. *J. Chem. Phys.* **1998**, *109*, 10180-10189.
- (90) Werner, H. J.; Knowles, P. J.; Manby, F. R.; Schütz, M.; Celani, P.; Knizia, G.; Korona, T.; Lindh, R.; Mitrushenkov, A.; Rauhut, G.;

Adler, T. B.; Amos, R. D.; Bernhardsson, A.; Berning, A.; Cooper, D. L.; Deegan, M. J. O.; Dobbyn, A. J.; Eckert, F.; Goll, E.; Hampel, C.; Hesselmann, A.; Hetzer, G.; Hrenar, T.; Jansen, G.; Köppl, C.; Liu, Y.; Lloyd, A. W.; Mata, R. A.; May, A. J.; McNicholas, S. J.; Meyer, W.; Mura, M. E.; Nicklass, A.; O' Neill, D. P.; Palmieri, P.; Pflüger, K.; Pitzer, R.; Reiher, M.; Shiozaki, T.; Stoll, H.; Stone, A. J.; Tarroni, R.; Thorsteinsson, T.; Wang, M.; Wolf, A. *MOLPRO*, version 2010.1, package of ab initio programs; see <http://www.molpro.net>.

- (91) Humphrey, W.; Dalke, A.; Schulten, K. VMD: visual molecular dynamics. *J. Mol. Graphics* **1996**, *14*, 33-38.
- (92) Rienstra-Kiracofe, J. C.; Tschumper, G. S.; Schaefer, H. F. III.; Nandi, S.; Ellison, G. B. Atomic and molecular electron affinities: photoelectron experiments and theoretical computations. *Chem. Rev.* **2002**, *102*, 231-282.
- (93) Ganteför, G. Photoelectron Spectroscopy. In *Quantum Phenomena in Clusters and Nanostructures*; Khanna, S. N.; Castleman, A. W. Jr., Eds.; 1st Edition; Springer-Verlag Berlin Heidelberg: New York, 2003.
- (94) Huang, X.; Zhai, H. J.; Kiran, B.; Wang, L. S. Observation of d-orbital aromaticity. *Angew. Chem. Int. Ed.* **2005**, *44*, 7251-7254.
- (95) Xie, L.; Li, W. L.; Romanescu, C.; Huang, X.; Wang, L. S. Photoelectron spectroscopy and density functional study of di-tantalum boride clusters: Ta B_x (x = 2-5). *J. Chem. Phys.* **2013**, *138*, 034308.
- (96) Li, H. F.; Kuang, X. Y.; Wang, H. Q. Probing structural and electronic properties of lanthanide-metal-doped silicon clusters: M@Si (M = Pr, Gd, Ho). *Phys. Lett. A* **2011**, *375*, 2836-2844.

Table 1. Relative Energies of Low-lying Isomers of Mo S / (n = 4-8) Clusters at B3LYP Level (E < 0.40 eV), and Comparisons with CCSD(T) Single-point Calculations at B3LYP Geometries

Table 2. Vertical Detachment Energies (VDEs) of Lowest-energy Mo S / (n = 4-8) Clusters and Selected Low-lying Isomers (E < 0.4 eV) at B3LYP Level

Table 3. Calculated Free Energy Differences (ΔG) for Proposed Reaction (Eq. 1) at B3LYP/H-BS Level of Theory

Fig. 1. Optimized structures for Mo S and Mo S . Bond lengths in angstroms (Å).

Fig. 2. Optimized structures for Mo S and Mo S . Bond lengths in angstroms (Å).

Fig. 3. Optimized structures for Mo S and Mo S . Bond lengths in angstroms (Å).

Fig. 4. Optimized structures for Mo S and Mo S . Bond lengths in angstroms (Å).

Fig. 5. Optimized structures for Mo S and Mo S . Bond lengths in angstroms (Å).

Fig. 6. (a) Frontier molecular orbitals for neutral Mo S ground state (Fig. 1b). (b) Frontier molecular orbitals for anionic Mo S ground state (Fig. 1g).

Fig. 7. (a) Frontier molecular orbitals for neutral Mo S ground state (Fig. 2a). (b) Frontier molecular orbitals for anionic Mo S ground state (Fig. 2c).

Fig. 8. (a) Frontier molecular orbitals for neutral Mo S ground state (Fig. 3a). (b) Frontier molecular orbitals for anionic Mo S ground state (Fig. 3b).

Fig. 9. (a) Frontier molecular orbitals for neutral Mo S ground state (Fig. 4a). (b) Selected frontier molecular orbitals for anionic Mo S ground state (Fig. 4d).

Fig. 10. (a) Selected frontier molecular orbitals for neutral Mo S ground state (Fig. 5a). (b) Selected frontier molecular orbitals for anionic Mo S ground state (Fig. 5c).

Fig. 11. Valence bond descriptions and numerical electron spin density (in |e|) for ground state of Mo S / clusters. Numerical spin density shown in parentheses.

Fig. 12. Simulated photoelectron spectra from ground states for Mo S (n = 4-8) clusters at B3LYP/H-BS level. Simulations performed by fitting distribution of calculated VDEs with unit-area Gaussian functions of 0.1 eV width.

Fig. 13. Calculated first vertical detachment energies (VDE) of Mo S (n = 4-8) as function of S content (n).

Note: Figure translations are in progress. See original paper for figures.

Source: ChinaXiv – Machine translation. Verify with original.